UNIVERSITY OF CALIFORNIA SAN DIEGO

Metal-Organic Frameworks as Low-k Gap Fill for Logic and RF

A Thesis submitted in partial satisfaction of the requirements
for the degree Master of Science

in

Materials Science and Engineering

by

Jacob Watson

Committee in charge:

Professor Andrew Kummel, Chair
Professor Prabhakar Bandaru
Professor William Trogler

2023

Copyright

Jacob Watson, 2023

All rights reserved.

The Thesis of Jacob Watson is approved, and it is acceptable in quality and form for publication on microfilm and electronically.

University of California San Diego

2023

DEDICATION

To my fellow lab mates.

Without them, I would not have learned half as much.

Because of them, my experience was twice as enjoyable.

TABLE OF CONTENTS

THESIS APPROVAL PAGE iii

DEDICATION iv

TABLE OF CONTENTS v

LIST OF FIGURES vi

LIST OF ABBREVIATIONS viii

ABSTRACT OF THE THESIS ix

INTRODUCTION 1

CHAPTER 1: METAL-ORGANIC FRAMEWORK (MOF) CONVERSION PROCESS 5

CHAPTER 2: GAP FILLING PERFORMANCE 16

REFERENCES 24

LIST OF FIGURES

Figure 1.1: Structure of ZIF-8 Composed of Zn ions linked by imidazole. Image is reprinted from *M. Bergaoui et al.* 2

Figure 1.2: Comparison diagram for potential ILDs as a function of their stiffness and dielectric constant. Image is reprinted from *Krishtab et al.* 4

Figure 1.3: ALD ZnO chamber diagram. Nitrogen purge gas is controlled by an MFC 5

Figure 1.4: ZIF-8 MOF conversion process diagram. Temperature is monitored by a thermocouple. 7

Figure 1.5: SEM images of planar ZIF-8 films using (a) 1 nm, (b) 3 nm, (c) 5 nm, and (d) 7 nm sacrificial ALD ZnO layer. 8

Figure 1.6: AFM images with line traces of planar ZIF-8 films using (a) 1 nm, (b) 3 nm, (c) 5 nm, and (d) 7 nm sacrificial ALD ZnO layer. 10

Figure 1.7: Illustration of planar ZIF-8 MOF conversion process. Experimental data displayed in Figure 1.2 and Figure 1.3 suggest that the threshold of sufficient ZnO exists at around 5 nm. 11

Figure 1.8: (a) Illustration for sample W30 in which four successive layers of 6nm of ZnO converted to ZIF-8 are deposited on silicon, accompanied by XRD data as compared to simulation for ZIF-8. 13

Figure 1.9: AFM images for planar ZIF-8 MOF films which were converted for either (a) 1 hour, (b) 2 hours, (c) 3 hours, or (d) 4 hours. 14

Figure 1.10: I-V curve for planar ZIF-8 MOF films before and after a dehydration process carried out in vacuum chamber at 120 °C for 1 hour. 15

Figure 1.11: 1 nm sacrificial ZnO layers converted to ZIF-8 using (a) 80 °C or (b) 160 °C ALD substrate temperature during the ZnO deposition process. 16

Figure 2.1: 22 nm of ALD ZnO deposited on a patterned trench substrate supplied by Applied Materials. ZnO layer is conformal across the variety of trenches which are 200nm in depth and range from 40 nm to 400 nm in width. 18

Figure 2.2: Planar SEM images (top) and Cross-sectional TEM images (bottom) for patterned trench substrates deposited with 5 successive layers of (a) 9 nm and (b) 5 nm sacrificial ZnO layers converted to ZIF-8. 20

Figure 2.3: Illustration of the limitation of the ZIF-8 trench filling process in which a diffusion barrier is formed, leaving residual ZnO along the bottom and walls of

trenches. 21

Figure 2.4: TEM-EELS spectra for a portion of a patterned trench sample deposited with 5 nm of ZnO converted to ZIF-8. 22

Figure 2.5: High magnification cross-sectional TEM images of the 40 nm wide trenches for ZIF-8 films which were converted from (a) 3 nm and (b) 1 nm of sacrificial ZnO. 1 nm of ZnO results in filling with no residual ZnO. 22

Figure 2.6: Cross-sectional TEM images of patterned trench substrates deposited with 1 nm of ZnO converted to ZIF-8. Accumulation of ZIF-8 growth at the corners of the trenches suggests the influence of capillary action. 24

Figure 2.6: Schematic diagrams reprinted for the filling behavior of trenches for copper **(a)** bottom-up super-fill and **(b)** reflow from *Friedrich et al.* and *Wheeler et al.* respectively 24

LIST OF ABBREVIATIONS

2-HmIM	2-methylimidizole
AFM	Atomic Force Microscopy
ALD	Atomic Layer Deposition
CVD	Chemical Vapor Deposition
EELS	Electron Energy Loss Spectroscopy
GDU	Gas Distribution Unit
MFC	Mass Flow Controller
MIM	Metal-Insulator-Metal
MOF	Metal-Organic Framework
OSG	Organosilanes
SE	Spectroscopic Ellipsometry
SEM	Scanning Electron Microscopy
TEM	Tunneling Electron Microscopy
XRD	X-Ray Diffraction
ZIF-8	Zeolitic Imidazolate Frameworks

ABSTRACT OF THE THESIS

Metal-Organic Frameworks as Low-k Gap Fill for Logic and RF

by

Jacob Watson

Master of Science in Materials Science and Engineering

University of California San Diego, 2023

Professor Andrew C. Kummel, Chair

Currently, there is an unmet need for a seamless metal interconnect gap-filling material which not only possesses low dielectric constant and sufficient mechanical strength but can also be grown plasma-free. Nanoporous metal-organic frameworks (MOFs), particularly zeolitic imidazolate frameworks (ZIFs) are an attractive option to meet this need because of their favored reported properties and ability to be deposited using a simple thermal

vapor process. Furthermore, they are a candidate to be used in the semi-damascene process because it is organic and easily etched. In this work, ZIF-8 metal-organic frameworks were converted by exposing an ALD ZnO film to the vapor of an organic linker, 2-HmIM. Experiments on planar substrates suggest a threshold for the sacrificial ZnO layer thickness in which the ZIF-8 crystal grains coalesce to form a coherent layer, before which only islands are formed, and after which crystals continue to ripen and increase roughness. The formation of a coherent layer constitutes a diffusion barrier which prevents further linker diffusion, resulting in a saturated ZIF-8 layer thickness, and excess ZnO being left unconverted at the bottom. These results are consistent with recent literature experiments.

Experiments in the deposition of ZIF-8 onto patterned trench substrates with varying aspect ratios revealed a limitation on the sacrificial ZnO thickness on the full conversion of the ZnO layer which is consistent with what is observed for films deposited on planar substrates. Full conversion of the ZnO in trenches was shown for sufficiently low sacrificial ZnO layers, which has not been explicitly displayed in literature experiments. Furthermore, the mechanism for ZIF-8 gap filling was revealed to be motivated by reflow in which surface diffusion is enhanced by capillary forces. The geometry and progression of the filling is visually similar to bottom-up superfill described previously for Cu electrodeposition. These results serve as a strong basis for low temperature, plasma-free, and seamless gap fill of high and low aspect ratio trenches.

INTRODUCTION

As the miniaturization of IC continues, there is a need for lower-k interlayer dielectrics (ILDs) which have thermal, mechanical, and electrical properties to disrupt even the current approaches to ILDs such as plasma deposited organosilanes (OSGs). Utilization of the semi-damascene process creates a need for vapor phase deposited ILDs of sub-100nm thickness which can achieve gap fill. One candidate for such a material is metal-organic frameworks (MOF's) which are formed from a reaction between a metal and organic precursor to create a microporous, crystalline material with an open fraction as high as 70%. *Krishtab et al.* illustrated the current landscape for advanced low-k dielectrics which could be used as ILDs as a function of their dielectric constant and Young's modulus as represented in Figure 1.2. MOFs, namely zeolitic imidazolate frameworks (ZIFs) are favorable with values of k (dielectric constant) of 2.2 and E (Young's modulus) of 3.4 GPa for ZIF-8, shown in Figure 1.1, which has the chemical formula C4H6N2Zn. *Krishtab et al.* obtained these measurements by a vapor-phase conversion process in which 5.8 nm of atomic layer deposited (ALD) ZnO was exposed to an organic linker in vacuum at 120 °C to produce 24 nm of MOF. Gap fill performance was also reported, in which the material successfully filled 45 nm wide trenches in a fork-fork capacitor. This demonstrated ZIF-8's ability to provide seamless, plasma-free gap fill. However, in this case, there was unconverted remaining ZnO at the bottom of the trenches. This called for further investigation and optimization of the MOF conversion process.

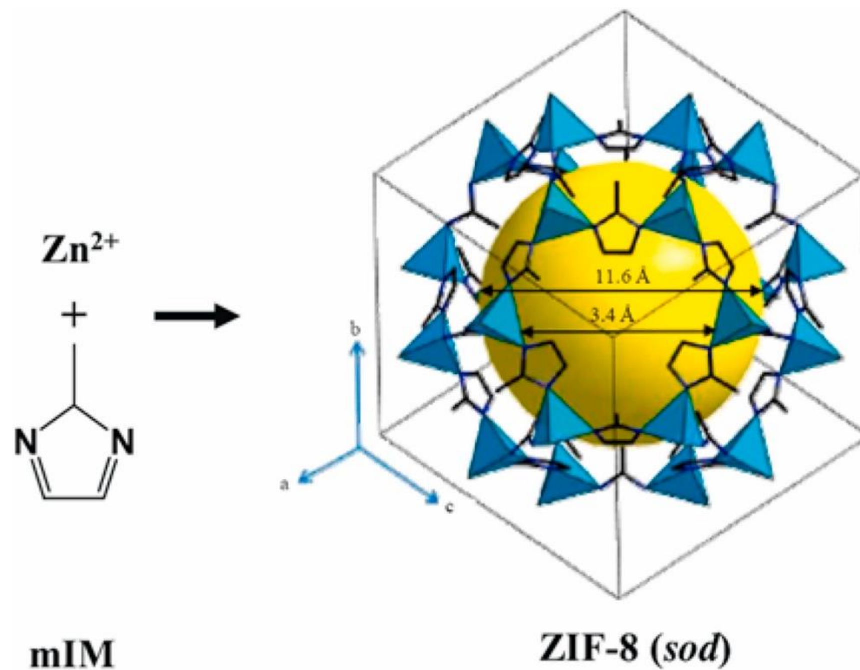

Figure 1.1: Structure of ZIF-8 composed of Zn ions linked by imidazole. Image is reprinted from *M. Bergaoui et al.*

Cruz et al. experimented with a custom MOF-CVD reactor for ZIF-8 in a cleanroom setting to examine scalability of the material. Key parameters such as process temperature, oxide thickness, and ligand exposure time in the ZnO to ZIF-8 conversion process were examined to obtain a uniform, pinhole free film on wafer. The group observed a conversion rate of 10x by using an ALD-ZnO layer of 3 nm and converting it to 30 nm which showed 4.4 nm root-mean-square (RMS) roughness at standard conditions. It was also concluded that a relative humidity of 12% resulted in island-growth ZIF-8 films 5x rougher than standard conditions.

Recently, *Kräuter et al.* investigated the impact of ZnO precursor density and conversion time on the thickness and morphology of resultant MOF films. The density of the plasma enhanced ALD deposited ZnO layer was varied by changing the interelectrodal distance. It was concluded that less dense ZnO layers always result in significantly rougher, nonconformal layers because it

converts faster, which is a similar mechanism induced by increased humidity. Also described is a clear saturation point in MOF layer thickness, which is highly dependent on the sacrificial ZnO layer. Additionally, increasing conversion time past the saturation point of thickness results in a slight increase in roughness due to crystal ripening.

The present work aimed to build upon the above studies and understand more about the ZnO to ZIF-8 conversion process, and how this conversion can be tailored and utilized most effectively in trenches for gap fill. The effect of varying the thickness of the sacrificial ZnO layer thickness on the structure of the resultant ZIF-8 film was characterized by planar and trench substrates. It was concluded that ZIF-8 crystal grains coalesce to form a coherent layer at a specific ZnO layer thickness, before which only islands are formed, and after which crystals continue to ripen and increase roughness. The formation of a coherent layer constitutes a diffusion barrier which prevents further linker diffusion Finally, the mechanism for ZIF-8 gap filling was revealed to behave as bottom-up superfill like that described previously for Cu electrodepsotiion, which is a key finding for gap filling applications.

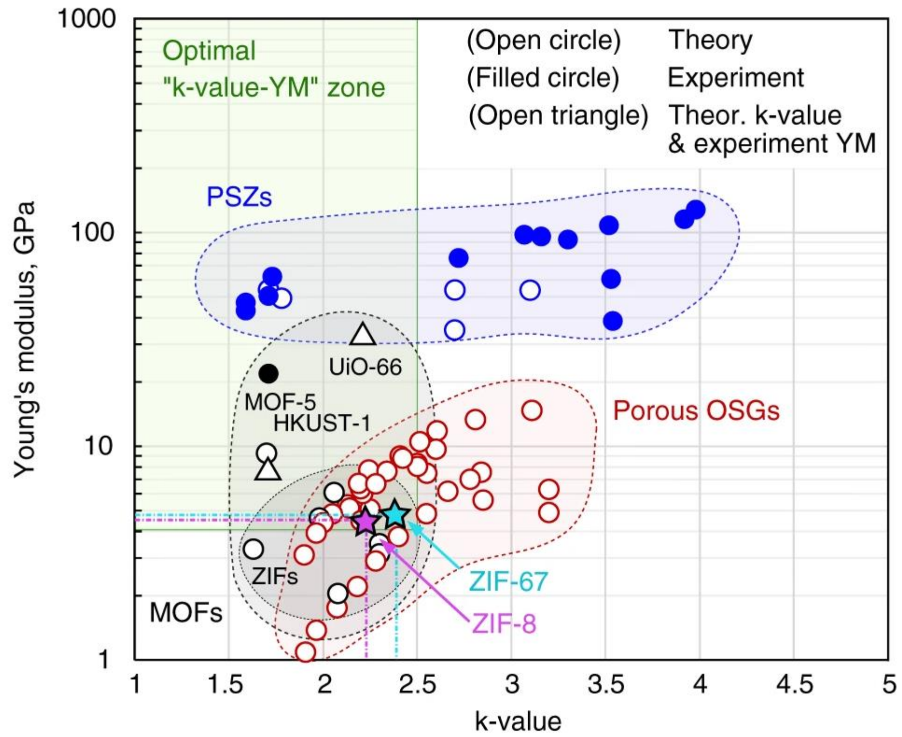

Figure 1.2: Comparison diagram for potential ILDs as a function of their stiffness and dielectric constant. Image is reprinted from *Krishtab et al.*

CHAPTER 1: METAL-ORGANIC FRAMEWORK (MOF) CONVERSION PROCESS

Depositing a film of the zeolitic imidazolate framework-8 (ZIF-8), which is a specific MOF, consists of exposing a layer of atomic layer deposited (ALD) zinc oxide (ZnO) to the vapor of organic linker 2-methylimidizole (2-HmIM) at a certain temperature for a fixed time. During this process, the ZnO is converted to ZIF-8 which is a microporous, crystalline material. The conversion results in the growth of grains and associated volume expansion. To control and optimize this conversion process, for applications such as gap fill, it is critical to understand the behavior. Conversion experiments were carried out utilizing a home-built ALD ZnO system as shown in Figure 1.3 to act as feedstock for MOF. The initial ZnO layer is thought of as the "sacrificial" layer in the MOF conversion process. Note that "MOF" in the present report is herein synonymous with the MOF ZIF-8.

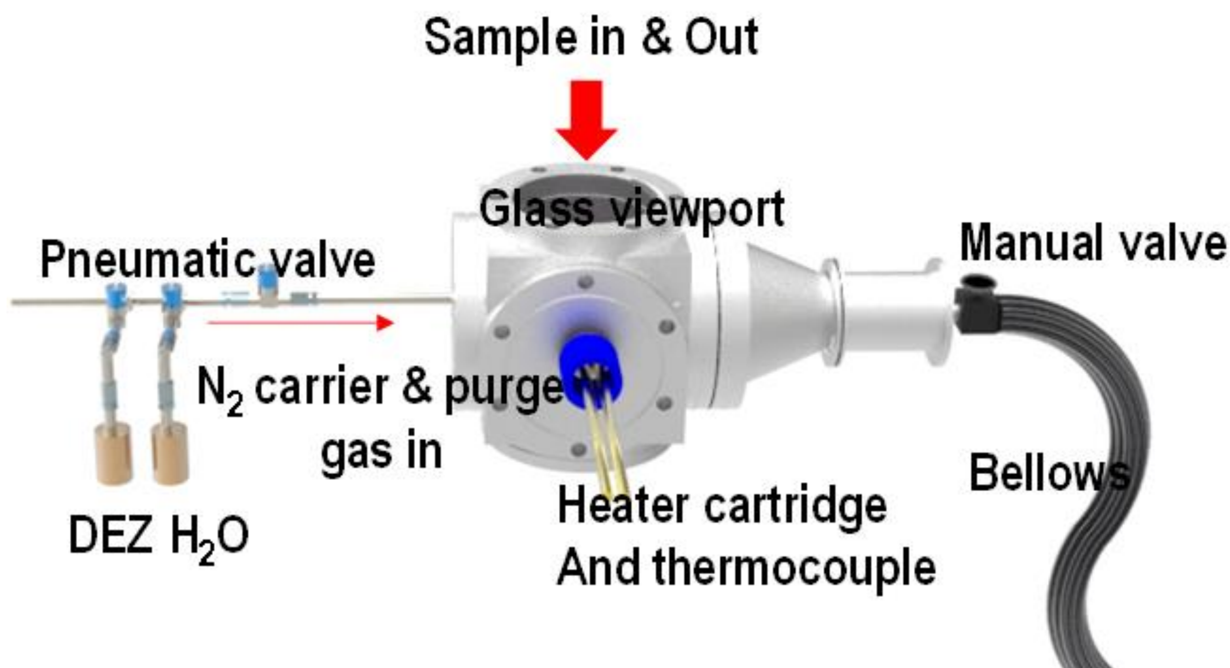

Figure 1.3: ALD ZnO chamber diagram. Nitrogen purge gas is controlled by an MFC.

A home-built ALD reactor was used for the ZnO layer deposition. The system consisted of a high-purity nitrogen line leading to a gas distribution unit (GDU) for the DEZ and H2O precursors. Nitrogen flow was controlled by a 50 sccm mass flow controller (MFC). The GDU leads directly into the load lock which is continuously pumped by a mechanical pump for a base pressure of 100 mTorr read by a Convectron pressure gauge. A ConFlat window on the load lock was sealed using a viton o-ring. Loading of a sample required venting the chamber at room temperature. Once loaded, the chamber was once again evacuated and heated by electrical heat tapes and a cartridge heater to heat the walls and substrate stage to 120°C and 80°C respectively by thermocouple reading. Once the temperature was stable, the MFC was set such that nitrogen purge pressure was 300 mTorr. With precursor valves open, two ALD valves controlled by a relay board and Arduino program delivered pulses of 150 ms and 400 ms for the DEZ and H2O respectively. Purge time was 20 s to fully pump out the chamber between cycles which is a result of the slow pump speed. After running the desired number of cycles at a growth rate of roughly 1.2 Å/cycle, the chamber was cooled to room temperature and vented to retrieve the sample.

Diethyl Zinc (DEZ) with min. 95% purity contained in 50 ml Swagelok cylinder was obtained from Strem Chemicals Inc. 99% pure 2-methylimidazole (2-HmIM) powder was obtained from Sigma-Aldrich. ACS Regents grade of acetone (99.5+ wt.%), methanol (99.5+ wt.%), deionized (DI) water (99.5+ wt.%), isopropyl alcohol (99.5+ wt.%), and hydrofluoric acid (HF) (48 wt.%) were purchased from Fisher Scientific. P-type Si substrates were provided by University Wafers were used for deposition of ZnO thin films as feedstock into the planar MOF conversion process. The p-type substrates were cleaned by swabbing with methanol to remove any particulates remnant from dicing procedure, then rising with methanol

and isopropyl alcohol, after which they were soaked in 2 wt.% HF solution for 5 minutes and finally blown dry with high-purity nitrogen. In Chapter 2, the MOF conversion process on 3D, patterned trench substrates will be described.

After ALD ZnO deposition, the samples were set face down on the open mouth of a glass vial with roughly 150 mg the organic linker 2-HmIM at the bottom, as illustrated in Figure 1.4. The samples were secured by double-sided Kapton tape. This vial was encapsulated by a larger vial which was sealed by a plastic screw-on lid. This entire system was placed inside an isothermal oven by Fisher Scientific in ambient conditions and heated to 115°C measured by a thermocouple. After 1-4 hours, the system was removed from the oven and the samples were placed in the sample holder. Vials used in the MOF conversion process were cleaned by rinsing and swabbing with acetone, and fresh linker and tape were used for each sample or cycle.

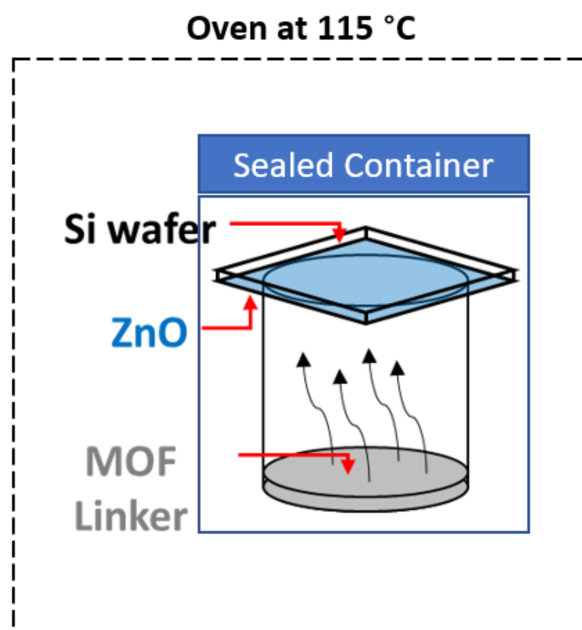

Figure 1.4: ZIF-8 MOF conversion process diagram. Temperature is monitored by a thermocouple.

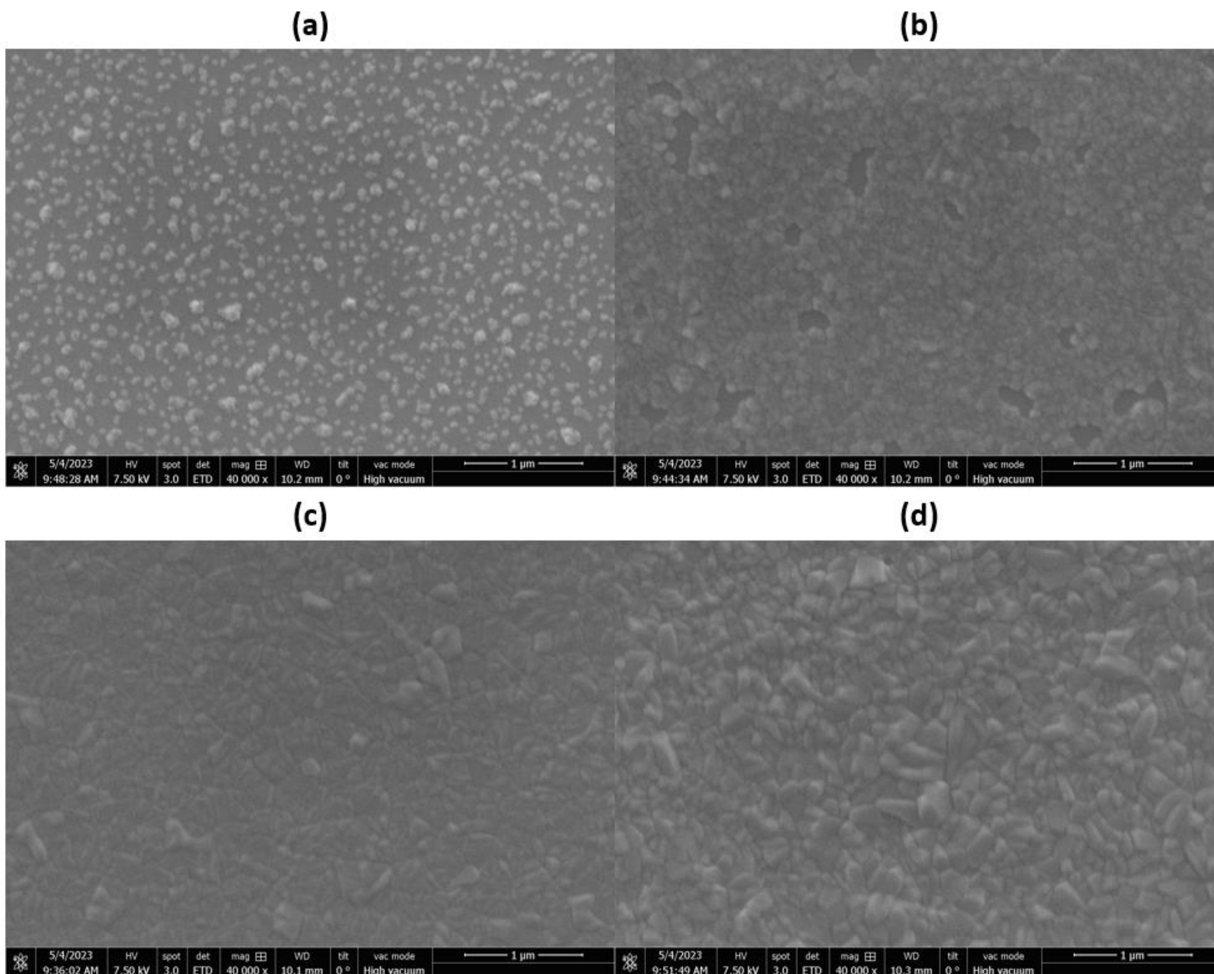

Figure 1.5: SEM images of planar ZIF-8 films using **(a)** 1 nm, **(b)** 3 nm, **(c)** 5 nm, and **(d)** 7 nm sacrificial ALD ZnO layer.

ZnO films of varying thickness were converted to ZIF-8 using the same process to determine how ZnO thickness influences the ZIF-8 conversion morphology and thickness. Figure 1.5 and Figure 1.6 display how the morphology and grain coalescence changes as a function of ZnO thickness for 1 nm, 3 nm, 5 nm, and 7 nm sacrificial ZnO layers using the surface characterization techniques scanning electron microscopy (SEM) and atomic force microscopy (AFM) respectively. AFM was carried out using the Park Systems model XE7 atomic force microscope by non-contact mode. SEM was carried out using the FEI Quanta 200 model scanning electron microscope in high vacuum mode at 5 keV. MOF samples were coated with

iridium using a sputter coater before SEM and attached to the stage with carbon tape. These sets of images clearly show a threshold of ZnO thickness in which the ZIF-8 crystal grains coalesce and form a coherent layer which exists at roughly 5 nm of ZnO.

The thickness of the films was determined by spectroscopic ellipsometry (SE) using the model M−2000D by J.A. Woollam Co., Inc. equipped with a focusing probe that reduced the spot size to 300–400 μm. The SE results were collected at incident angles of 75°. SE data was fitted using two different models using the CompleteEase software: Si substrates with either a transparent (Cauchy) or absorbing (B-Spline) layer for the ZnO and ZIF-8 respectively. However, experiments on the various film morphologies suggested that the SE measurements were consistently overestimating the thickness due to the high roughness of the films. From AFM data described in Figure 1.6, the grain growth and coalescence only form a layer which is around 40 nm in thickness, which is saturated from the formation of a diffusion barrier against the organic linker vapor.

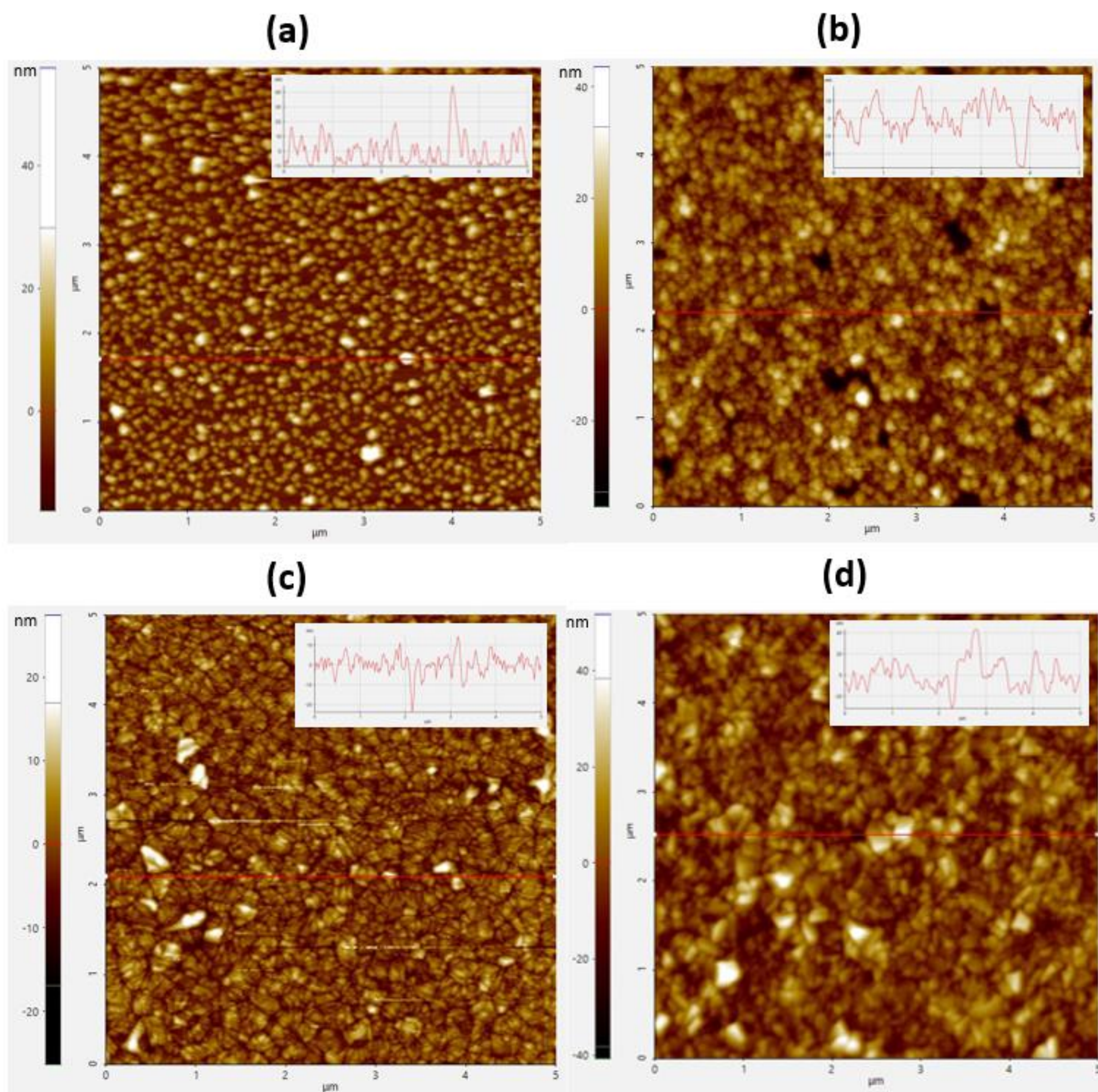

Figure 1.6: AFM images with line traces of planar ZIF-8 films using **(a)** 1 nm, **(b)** 3 nm, **(c)** 5 nm, and **(d)** 7 nm sacrificial ALD ZnO layer. RMS roughness values are 7.6 nm, 8.38 nm, 4.32 nm, and 9.77 nm respectively.

Figure 1.7 specifically describes the conclusion that sacrificial ZnO below the threshold amount for coalescence results in island growth dominated by the phenomenon of Ostwald ripening. Nucleated grains arrest the adjacent MOF nucleation from ZNO when introduced to more organic linker vapor, such that the film is incoherent with large voids. Once a coherent layer is formed , any additional MOF formation results in further ripening of the crystal grains,

resulting in a rougher surface as well as residual ZnO at the bottom. The saturation of the conversion and ripening of the top grains is caused by the formation of a diffusion barrier once the grains have coalesced which prevents the 2-HmIM linker from reaching the ZnO at the bottom.

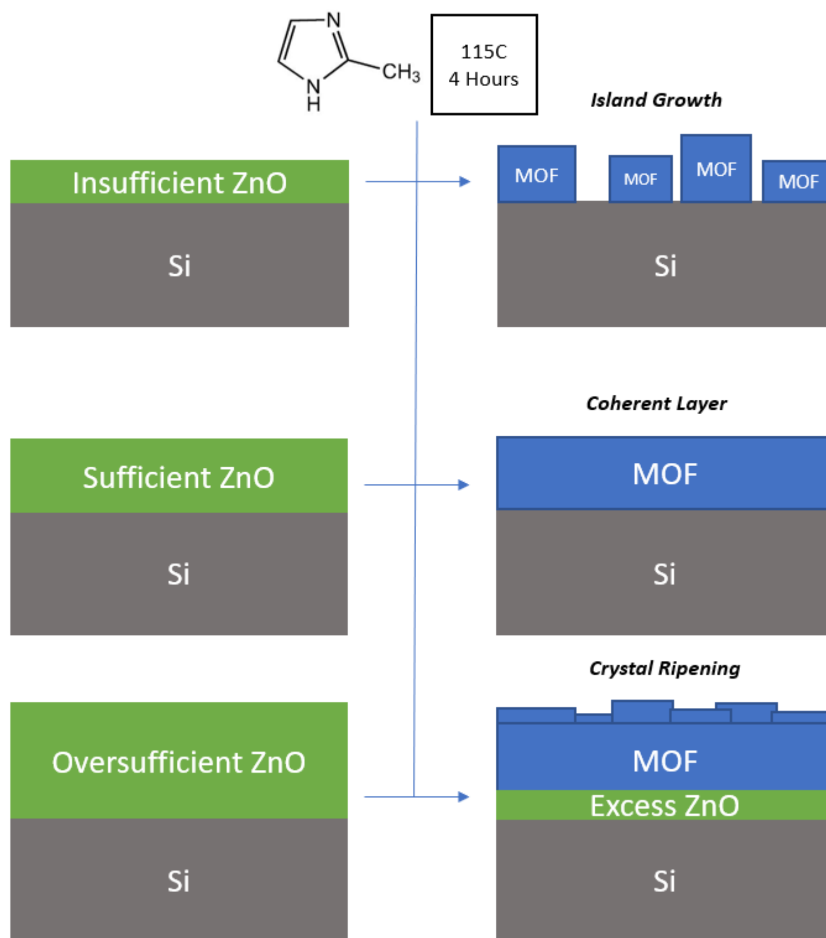

Figure 1.7: Illustration of planar ZIF-8 MOF conversion process. Experimental data displayed in Figure 1.5 and Figure 1.6 suggest that the threshold of sufficient ZnO exists at around 5 nm.

Electrical properties of the ZIF-8 films are critical for application as a gap fill material since it must be electrically insulating with a low dielectric constant. As described above, literature has shown that ZIF-8 films can yield a dielectric constant of 2.2. To observe the electrical properties of the as-deposited ZIF-8, a film consisting of four successive layers of 6 nm of ZnO converted

to ZIF-8 was made. Excessive thickness of roughly 200 nm was the objective so that leakage would be sufficiently low for an accurate capacitance measurement, as well as permitting the ability to measure accurate x-ray diffraction data, since crystallinity is closely related to dielectric properties.

Figure 1.8 describes this film and its crystallinity, morphology (AFM), and capacitance. Crystallinity of the MOF material was determined by X-Ray Diffraction (XRD) using the Bruker D8 Advance. Capacitance was measured by depositing nickel dots on to top surface and gold on the back of the silicon substrate as the back contact. C-V measurements were carried out using a probe station to yield a calculated dielectric constant value of 5.1 considering the area of the nickel dots as well as the contribution of the 1.5 nm SiO2 layer on the substrate. Crystallinity agreed well with the ZIF-8 simulated diffraction pattern, with less intense peaks. Morphology was rough with RMS roughness estimates in a 1 x 1 um area to be roughly 20 nm, suggesting that the iterative layers of ZIF-8 resulted in a composite roughness equal to that of the sum of the individual layers. It was hypothesized that this roughness was significant enough to affect the capacitance value and therefore the dielectric constant.

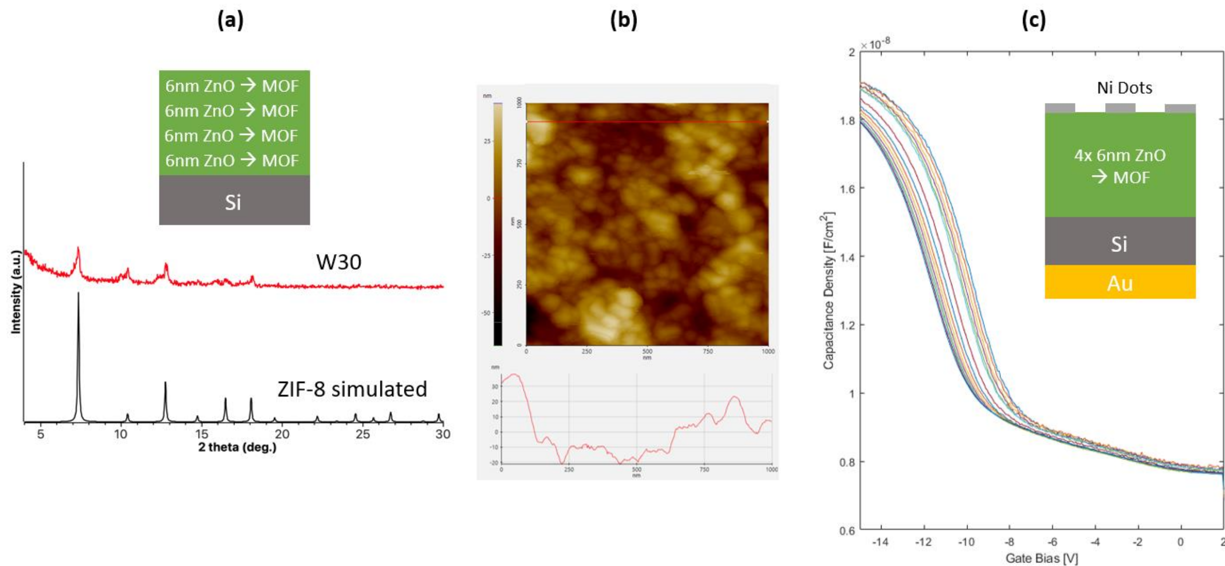

Figure 1.8: **(a)** Illustration for sample W30 in which four successive layers of 6nm of ZnO converted to ZIF-8 are deposited on silicon, accompanied by XRD data as compared to simulation for ZIF-8. Then film is roughly 200 nm as measured by SE, which is likely an overestimate due to high rouhgness. **(b)** AFM image of sample W30 with RMS roughness of 20.8 nm. **(c)** C-V curve for sample W30 which was made into an MIM capacitor shown by illustraion. Calculated dielectric constant was 5.1.

Total conversion time was hypothesized to be a variable that would impact the morphology of the resultant ZIF-8 film as well as the thickness. Four 7 nm ZnO samples were simultaneously deposited and converted for different conversion times for 1, 2, 3, and 4 hours. Figure 1.9 relays the AFM results of these four films after conversion, suggesting that RMS roughness increases with increasing conversion time. SE data was checked against the AFM data for these four films, and agreed with the conclusion that after 2 hours, the thickness saturated at around 40 nm.

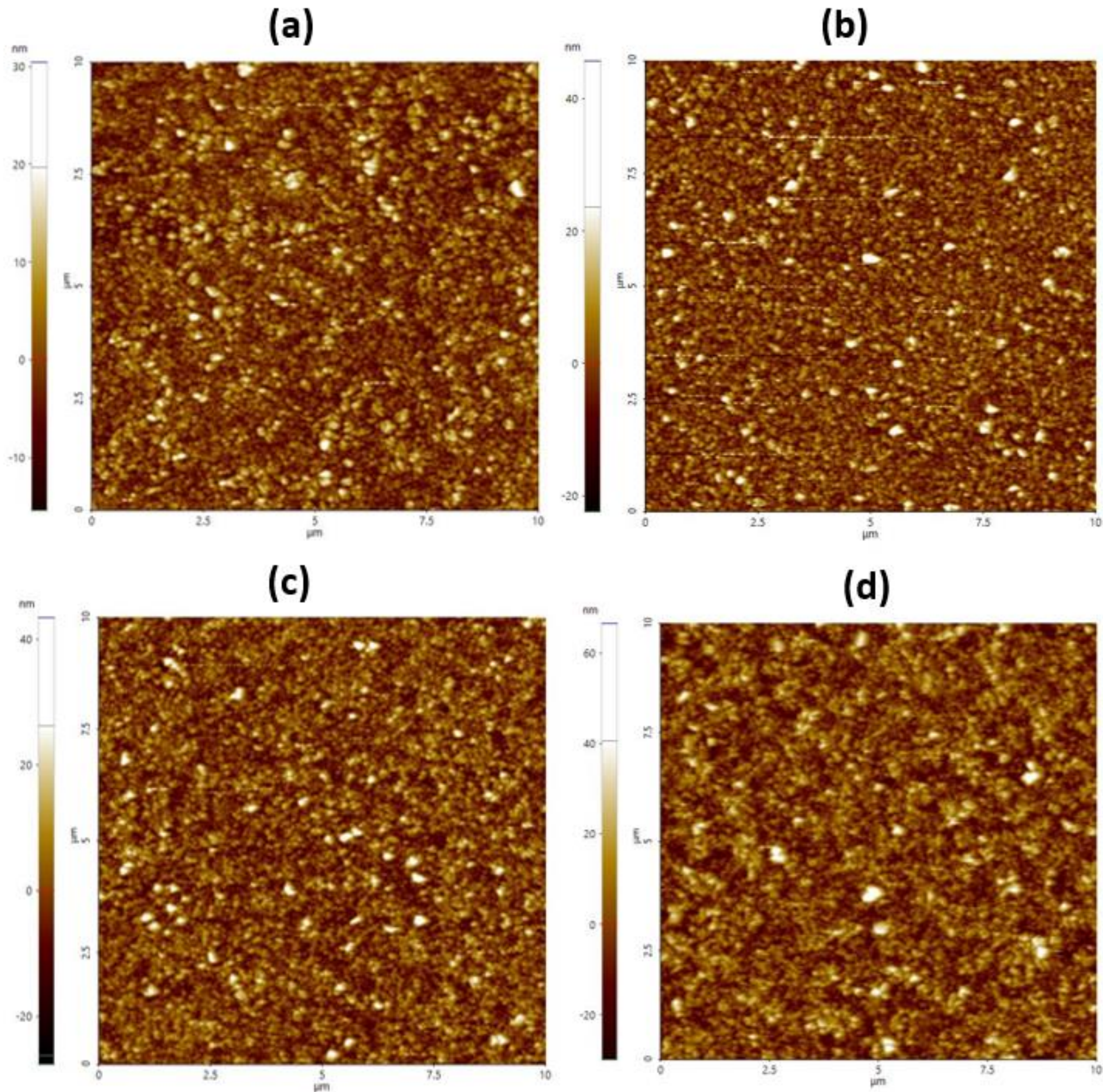

Figure 1.9: AFM images for planar ZIF-8 MOF films which were converted for either (a) 1 hour, (b) 2 hours, (c) 3 hours, or (d) 4 hours. RMS roughness values are 5.03 nm, 6.04 nm, 6.71 nm, and 10.33 nm respectively. Sacrificial ZnO layers were the same among the four films and had a thickness of 7 nm.

Films (b) and (c) from Figure 1.9 which correspond to the 7 nm ZnO films converted to ZIF-8 for 2 and 3 hours respectively were made into metal-insulator-metal (MIM) capacitors to observe whether measured dielectric constant would be lower for these smoother films. These capacitors used platinum electrodes rather than the nickel from Figure 1.9 to ensure minimal

diffusion of the dot material. Leakage was low enough for these films to permit capacitance measurement by the probe station, which resulted again in a dielectric constant of around 5 for both films. It was hypothesized that due to the porosity of the ZIF-8 material, some percentage of water could have diffused into the film during the significant periods of time between deposition and measurement. To ensure that the presence of water was not increasing the dielectric properties of the film, a dehydration procedure was carried out for the same two capacitors. The capacitors were dried in vacuum at 120 °C for 1 hour and remeasured for capacitance and leakage current. Capacitance for the two films remained the same, but leakage, however, decreased by roughly two orders of magnitude as shown in Figure 1.10. This result suggested that there was residual water embedded in the ZIF-8 film caused by ambient conversion conditions.

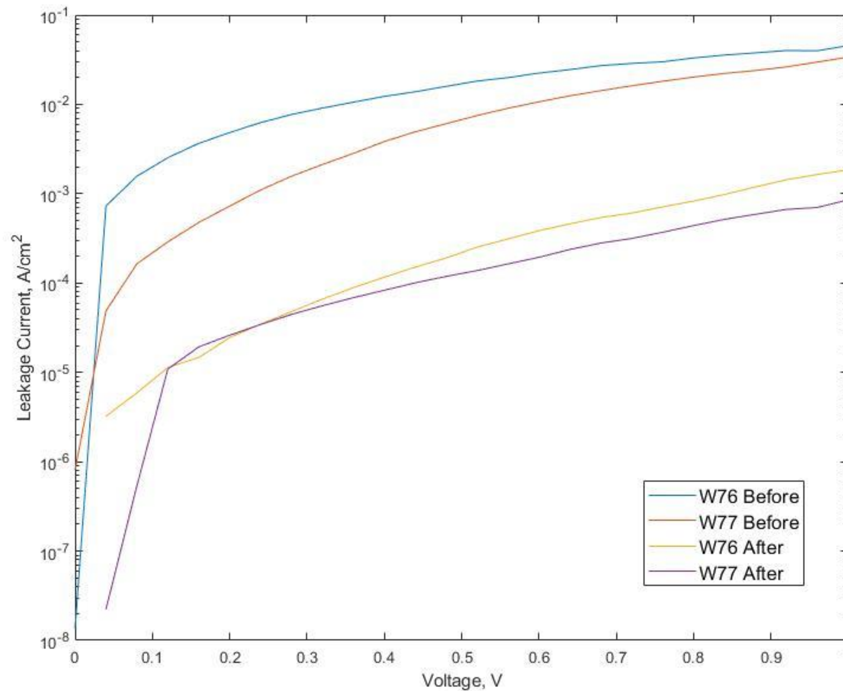

Figure 1.10: I-V curve for planar ZIF-8 MOF films before and after a dehydration process carried out in vacuum chamber at 120 °C for 1 hour. Sample W76 and W77 correspond to the samples (b) and (c) shown in Figure 1.9. A roughly two orders of magnitude decrease in leakage current is observed for both samples.

The consistently high k-value of the ZIF-8 films raised the question of crystallinity and its effect on dielectric properties. One of the largest influences on crystallinity of the ALD ZnO is the temperature of the substrate during deposition. The standard procedure for the ZnO deposition as described above used a temperature of 80 °C. This is considered low temperature deposition and is well known to produce films which are less crystalline. This was set according to the hypothesis that a more amorphous ZnO film is more reactive, and therefore would produce more ZIF-8 conversion. This hypothesis was thought to be realized by previous experiments but has since been questioned because the data relied on SE without morphology characterization that were likely skewed due to surface roughness and voids. Thus, a higher temperature ZnO substrate temperature of 160 °C was directly tested against 80 °C for the conversion of a 1 nm ZnO film. The surface morphology of these two films is described in Figure 1.11, which shows that 160 °C results in slightly more uniform and crystalline grains. This result suggested that more crystalline ZnO may result in more crystalline ZIF-8, and therefore a lower dielectric constant.

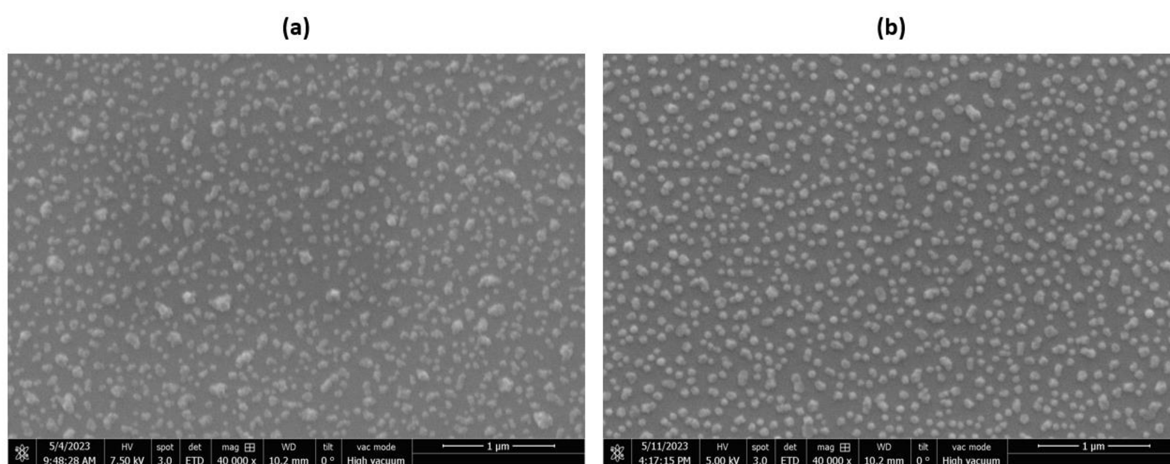

Figure 1.11: 1 nm sacrificial ZnO layers converted to ZIF-8 using **(a)** 80 °C or **(b)** 160 °C ALD substrate temperature during the ZnO deposition process.

CHAPTER 2: GAP FILLING PERFORMANCE

The objective application of the ZIF-8 material is for use as a low dielectric constant gap filling material, made possible by its mechanical and electrical properties, but primarily by its volume expansion capacity. The deposition process is also favorable because it is low temperature, plasma free, and theoretically seamless. Patterned Si substrates with trenches were obtained from Applied Materials for gap fill experiments. The trenches were 200 nm in depth and ranged in width from 40 nm to 400 nm such that a variety of aspect ratios could be tested. The only difference in deposition procedure between the trench substrates and the planar substrates are that the trench substrates were only blown dry before ZnO deposition with no HF cleaning or degreasing. Before any ZIF-8 conversion onto the patterned substrates, a thick layer of ZnO was deposited to validate the conformality of the ALD onto the trench features. Figure 2.1 shows a 22 nm thick layer of ZnO deposited on a patterned substrate with varying trench widths. The layer is conformal across all features, and there is a clear seam in the smallest 40 nm wide trenches which validates the growth rate is the same as planar samples, since the growth from each wall would be roughly 20 nm.

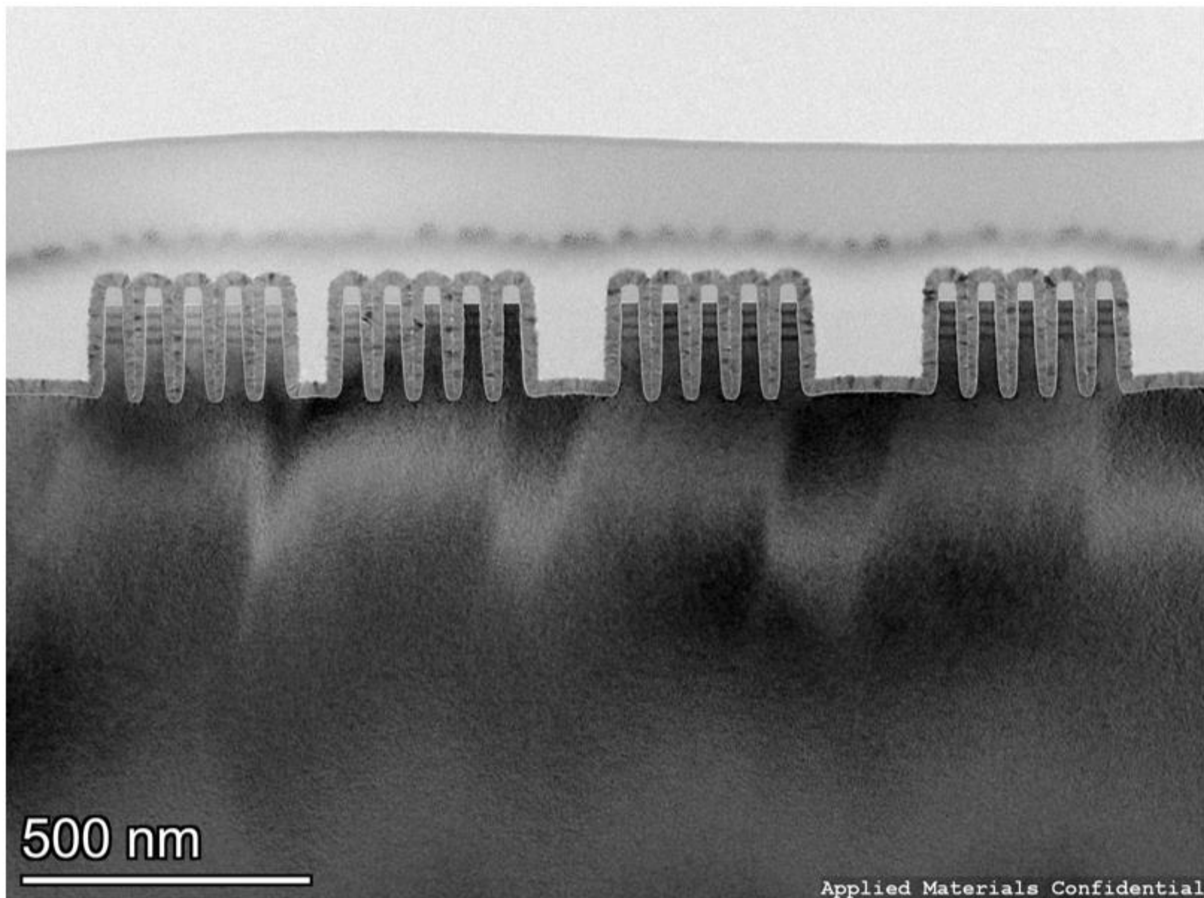

Figure 2.1: 22 nm of ALD ZnO deposited on a patterned trench substrate supplied by Applied Materials. ZnO layer is conformal across the variety of trenches which are 200nm in depth and range from 40 nm to 400 nm in width. See Figure 2.4 for breakdown of substrate material structure.

The first ZIF-8 trench sample tested consisted of 5 iterative layers of 9 nm ALD ZnO converted to ZIF-8. This sample is shown in Figure 2.2(a) from a planar SEM image and a cross-sectional TEM image. From the cross-section, 5 distinct layers of residual ZnO are clearly seen, in which some ZnO depositions were thicker or thinner depending on experimental consistency. There is no observable seam between the trenches. By observing the average thickness between the layers of residual ZnO, the roughly 40 nm limit for conversion due to the formation of a diffusion barrier hypothesis is validated. A thick residual ZnO layer at the bottom of the trenches

is also observed, which is detrimental to the performance of ZIF-8 as a deposition process for gap fill because the ZnO is slightly conductive and connects the metal interconnect lines.

A thinner version of this sample, with 5 iterative layers of 5 nm ZnO converted to ZIF-8 is shown in Figure 2.2(b). The cross-sectional TEM shows no distinct residual ZnO layers for the layers after the first, meaning total conversion of the ZnO; however, the residual ZnO remains from the first layer at the bottom. This result suggests a phenomenon preventing full conversion of the first layer in the trenches. Since there is clearly less residual ZnO from the 5 nm sacrificial ZnO layer than for 9 nm, it was hypothesized that moving to thinner and thinner sacrificial ZnO layers may shed light on the mechanism of gap fill relative to the ZnO thickness.

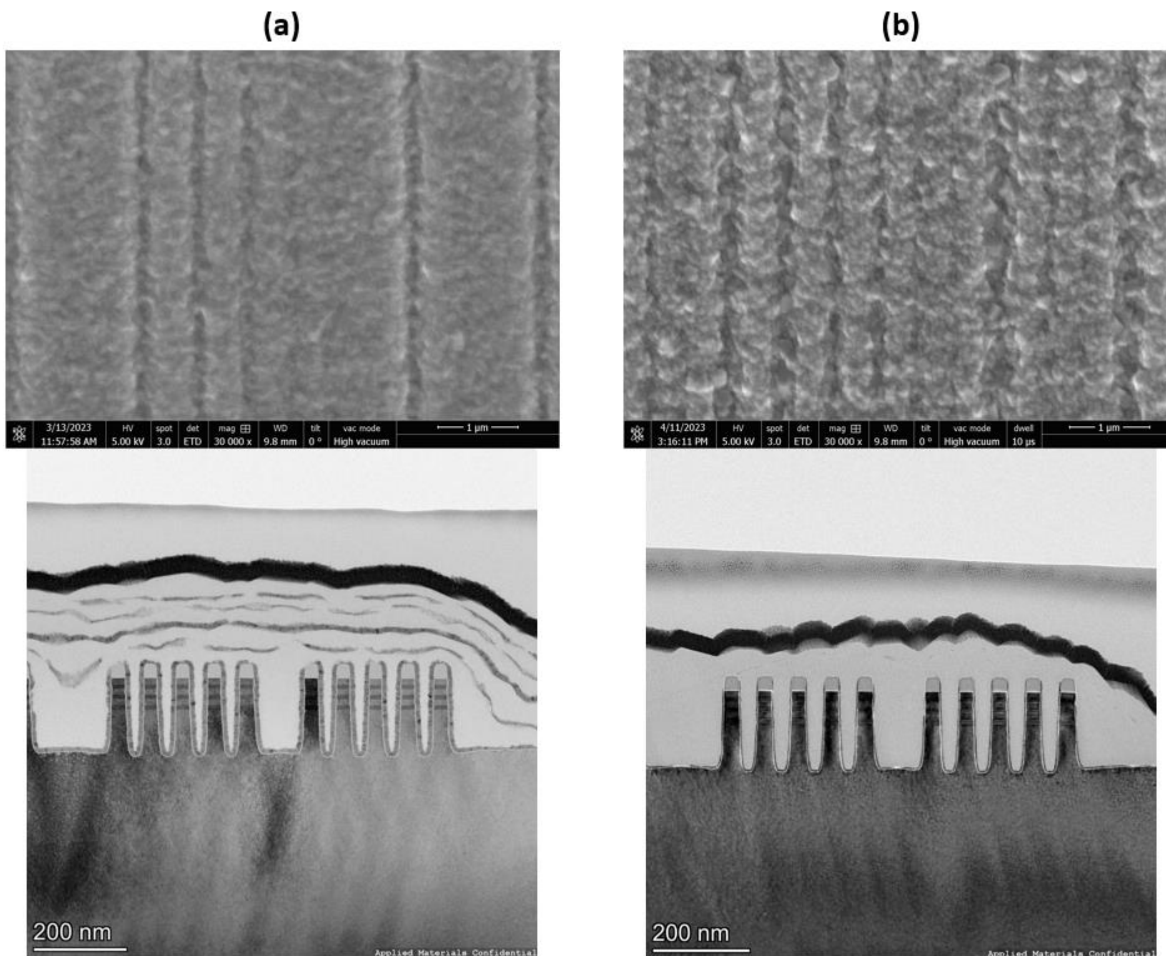

Figure 2.2: Planar SEM images (top) and Cross-sectional TEM images (bottom) for patterned trench substrates deposited with 5 successive layers of (a) 9 nm and (b) 5 nm sacrificial ZnO layers converted to ZIF-8. Bright regions represent ZIF-8 and dark stripes represent residual ZnO. Samples are coated with sputtered iridium for the SEM imaging process which appears black in cross-section.

Figure 2.3 illustrates a model for the mechanism of ZIF-8 trench fill which results in residual ZnO at the bottom of the trenches. Since the trenches have contributions of conversion from both the walls and the bottom, conversion is accelerated, and once the trench has been closed, or a coherent layer formed, then the linker can no longer convert the ZnO remaining at the bottom of the trench. This is consistent with the ZIF-8 film growth behavior on planar substrates, however happens at an accelerated rate in the narrow trenches due to the combination of ZIF-8 contributions from the wall and bottom.

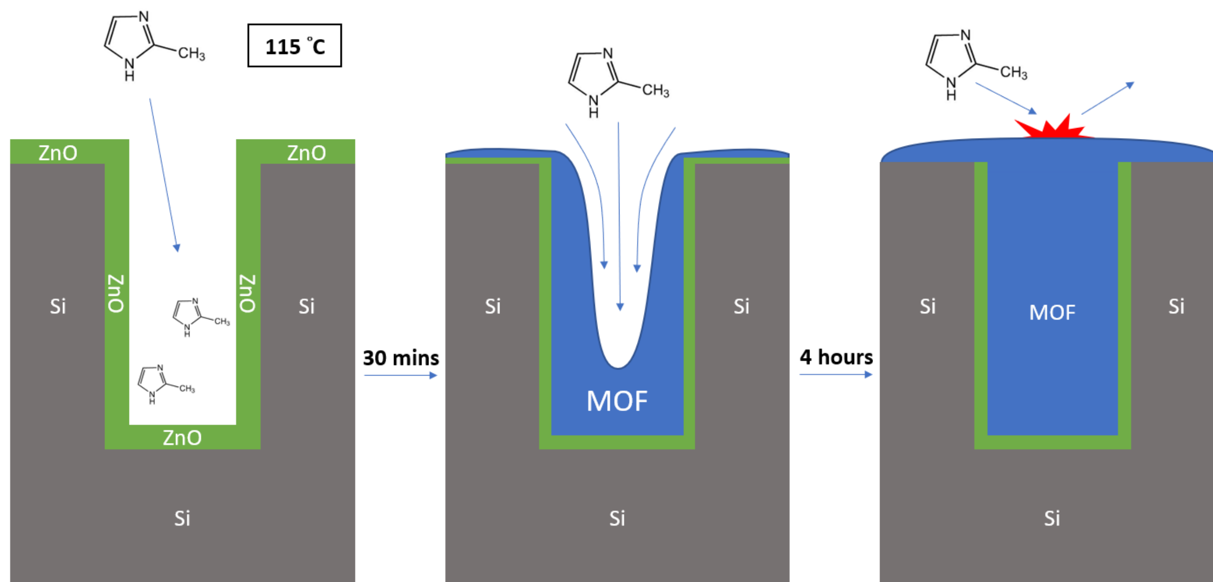

Figure 2.3: Illustration of the limitation of the ZIF-8 trench filling process in which a diffusion barrier is formed, leaving residual ZnO along the bottom and walls of trenches.

To ensure that it was ZnO at the bottom of the trenches, and that it is indeed a coherent film of ZIF-8 filling the trench, a TEM-EELS measurement was taken to see chemical distribution. Figure 2.4 shows the elements existing at a specific trench, in which ZnO is shown to be partially converted. This result is consistent with the model shown in Figure 2.3, because the side walls still contain ZnO after the trench had been closed with ZIF-8, but the tips of the trenches can still be exposed to organic linker vapor. This image also shows the structure of the substrate trenches themselves, consisting of layers of Si and SiGe, then topped with SiN. Finally, in the bright regions, the chemical composition of ZIF-8 is validated except for the apparent lack of a carbon signal. Carbon makes up a significant amount of ZIF-8 and should be shown. This lack of signal could possibly be due to an error in measurement since EELS is very sensitive to user input.

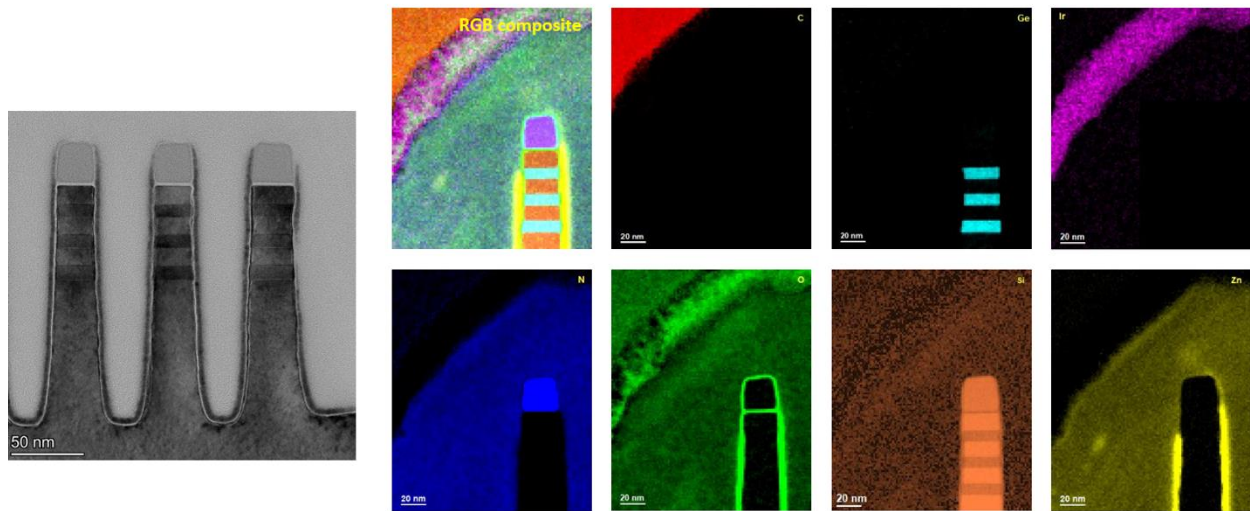

Figure 2.4: TEM-EELS spectra for a portion of a patterned trench sample deposited with 5 nm of ZnO converted to ZIF-8.

To obtain gap fill without residual ZnO, trench samples with 3 nm and 1 nm of sacrificial ZnO layers were converted to ZIF-8 on the patterned substrates. High magnification cross-sectional TEM images of these two samples are shown in Figure 2.5. The 3 nm ZnO sample has clear residual ZnO, similar in magnitude to the 5 nm ZnO sample. The 1 nm ZnO sample, however, shows no signs of a residual ZnO layer.

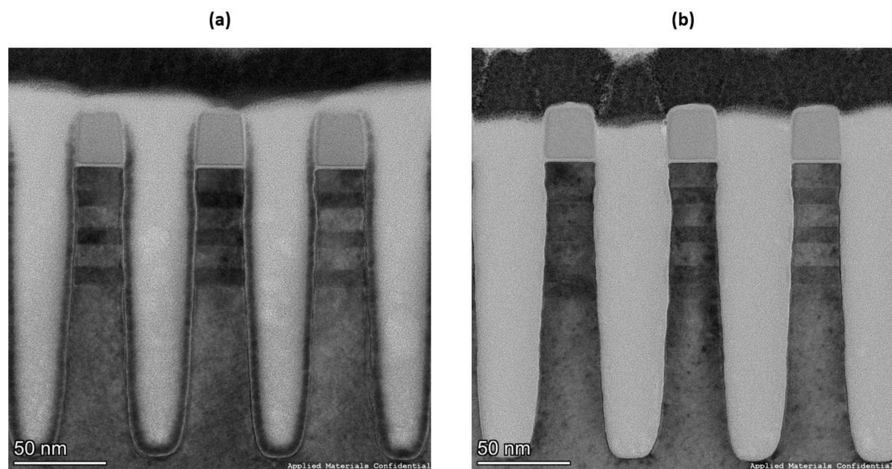

Figure 2.5: High magnification cross-sectional TEM images of the 40 nm wide trenches for ZIF-8 films which were converted from **(a)** 3 nm and **(b)** 1 nm of sacrificial ZnO. 1 nm of ZnO results in filling with no residual ZnO.

Figure 2.6 displays the 1 nm ZnO trench sample at lower magnification to observe a range of aspect ratios. These images shed light on the mechanism of the ZIF-8 trench fill, in which the ZIF-8 tends to accumulate at the corners of the trenches to maximize surface area with respect to volume, suggesting a phenomenon like capillary action. The reflow property of ZIF-8 trench fill is consistent with the apparent bottom-up and self-leveling filling described in Figure 2.7 for previous literature experiments with copper trench filling by electrodeposition with angles at the bottom, and eventual overfilling at the top. Layers of 1 nm ZnO converted to ZIF-8 could be iteratively deposited to fill trenches of varying depth. Future experiments should test this hypothesis to observe how the trenches fill in during successive layers after being filled completely. Another experiment of interest would be to examine whether the harsh iridium sputtering could induce any of the effects seen in the TEM images. An ALD deposited aluminum oxide layer could protect the ZIF-8 film and validate the filling mechanism. Finally, the difference between atmospheric and vacuum condition conversion processes should be characterized in order to confirm if the dielectric constant of ZIF-8 films converted in atmospheric conditions is higher than vacuum conditions due to the presence of water in the film.

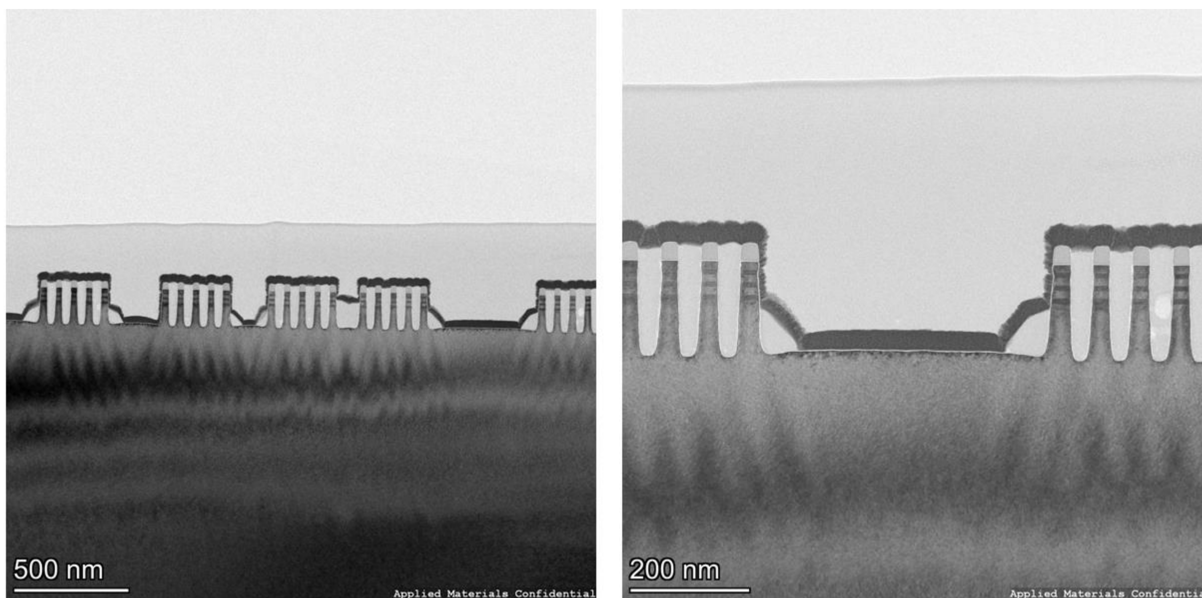

Figure 2.6: Cross-sectional TEM images of patterned trench substrates deposited with 1 nm of ZnO converted to ZIF-8 at two magnifications. Accumulation of ZIF-8 growth at the corners of the trenches suggests the influence of capillary action. Bottom-up filling and overfilling of the trenches is like behavior of copper electrodeposition.

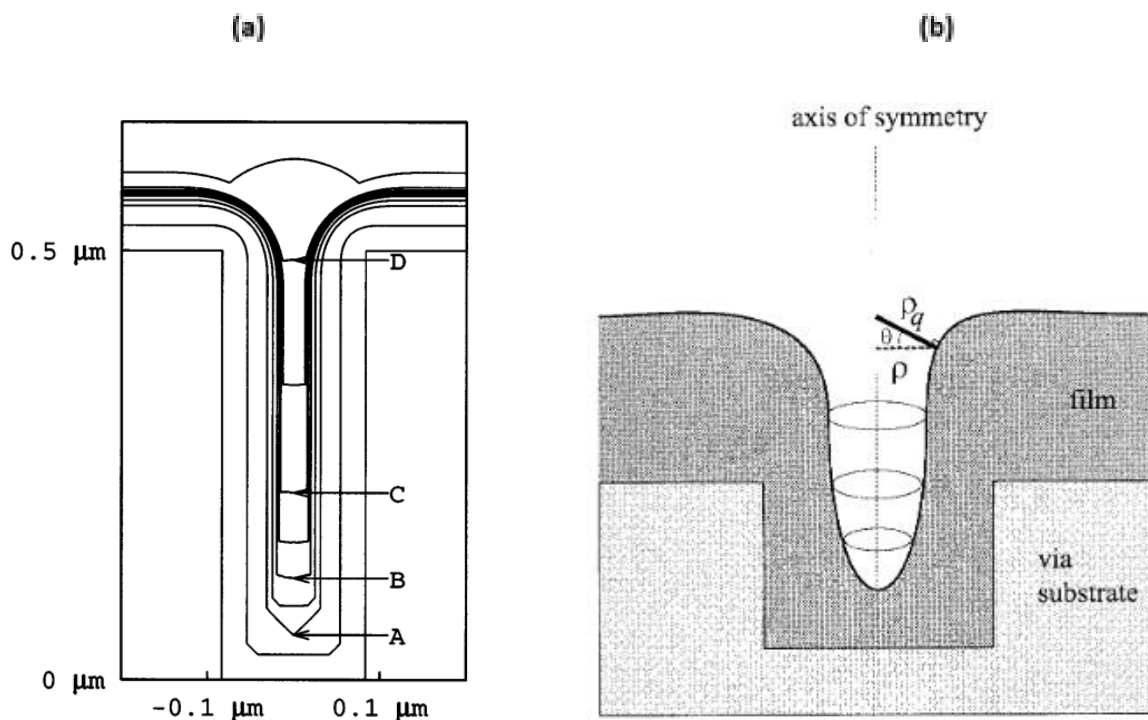

Figure 2.7: Schematic diagrams reprinted for the filling behavior of trenches for copper **(a)** bottom-up super-fill and **(b)** reflow from *Friedrich et al.* and *Wheeler et al.* respectively.

REFERENCES

[1] Allegretto, J. A.; Arcidiácono, M.; Steinberg, P. Y.; Angelomé, P. C.; Azzaroni, O.; Rafti, M. Impact of Chemical Primers on the Growth, Structure, and Functional Properties of ZIF-8 Films. *J. Phys. Chem. C* **2022**, *126* [15], 6724–6735. https://doi.org/10.1021/acs.jpcc.1c10425.

[2] Allendorf, M. D.; Dong, R.; Feng, X.; Kaskel, S.; Matoga, D.; Stavila, V. Electronic Devices Using Open Framework Materials. *Chem. Rev.* **2020**, *120* [16], 8581–8640. https://doi.org/10.1021/acs.chemrev.0c00033.

[3] Bergaoui, M.; Khalfaoui, M.; Awadallah-F, A.; Al-Muhtaseb, S. A Review of the Features and Applications of ZIF-8 and Its Derivatives for Separating CO2 and Isomers of C3- and C4- Hydrocarbons. *Journal of Natural Gas Science and Engineering* **2021**, *96*, 104289. https://doi.org/10.1016/j.jngse.2021.104289.

[4] Bétard, A.; Fischer, R. A. Metal–Organic Framework Thin Films: From Fundamentals to Applications. *Chem. Rev.* **2012**, *112* [2], 1055–1083. https://doi.org/10.1021/cr200167v.

[5] Crivello, C.; Sevim, S.; Graniel, O.; Franco, C.; Pané, S.; Puigmartí-Luis, J.; Muñoz-Rojas, D. Advanced Technologies for the Fabrication of MOF Thin Films. *Mater. Horiz.* **2021**, *8* [1], 168–178. https://doi.org/10.1039/D0MH00898B.

[6] Cruz, A. J.; Stassen, I.; Krishtab, M.; Marcoen, K.; Stassin, T.; Rodríguez-Hermida, S.; Teyssandier, J.; Pletincx, S.; Verbeke, R.; Rubio-Giménez, V.; Tatay, S.; Martí-Gastaldo, C.; Meersschaut, J.; Vereecken, P. M.; De Feyter, S.; Hauffman, T.; Ameloot, R. Integrated Cleanroom Process for the Vapor-Phase Deposition of Large-Area Zeolitic Imidazolate Framework Thin Films. *Chem. Mater.* **2019**, *31* [22], 9462–9471. https://doi.org/10.1021/acs.chemmater.9b03435.

[7] Eslava, S.; Zhang, L.; Esconjauregui, S.; Yang, J.; Vanstreels, K.; Baklanov, M. R.; Saiz, E. Metal-Organic Framework ZIF-8 Films As Low-κ Dielectrics in Microelectronics. *Chem. Mater.* **2013**, *25* [1], 27–33. https://doi.org/10.1021/cm302610z.

[8] Friedrich, L. J.; Dew, S. K.; Brett, M. J.; Smy, T. A Simulation Study of Copper Reflow Characteristics in Vias. *IEEE Trans. Semicond. Manufact.* **1999**, *12* [3], 353–365. https://doi.org/10.1109/66.778203.

[9] Furukawa, H.; Cordova, K. E.; O'Keeffe, M.; Yaghi, O. M. The Chemistry and Applications of Metal-Organic Frameworks. *Science* **2013**, *341* [6149], 1230444. https://doi.org/10.1126/science.1230444.

[10] Kräuter, M.; Cruz, A. J.; Stassin, T.; Rodríguez-Hermida, S.; Ameloot, R.; Resel, R.; Coclite, A. M. Influence of Precursor Density and Conversion Time on the Orientation of Vapor-Deposited ZIF-8. *Crystals* **2022**, *12* [2], 217. https://doi.org/10.3390/cryst12020217.

[11] Krishtab, M.; Stassen, I.; Stassin, T.; Cruz, A. J.; Okudur, O. O.; Armini, S.; Wilson, C.; De Gendt, S.; Ameloot, R. Vapor-Deposited Zeolitic Imidazolate Frameworks as Gap-Filling Ultra-Low-k Dielectrics. *Nat Commun* **2019**, *10* [1], 3729. https://doi.org/10.1038/s41467-019-11703-x.

[12] Lehmann, D.; Seidel, F.; Zahn, D. R. Thin Films with High Surface Roughness: Thickness and Dielectric Function Analysis Using Spectroscopic Ellipsometry. *SpringerPlus* **2014**, *3* [1], 82. https://doi.org/10.1186/2193-1801-3-82.

[13] Maex, K.; Baklanov, M. R.; Shamiryan, D.; Lacopi, F.; Brongersma, S. H.; Yanovitskaya, Z. S. Low Dielectric Constant Materials for Microelectronics. *Journal of Applied Physics* **2003**, *93* [11], 8793–8841. https://doi.org/10.1063/1.1567460.

[14] Oh, H.; Kim, J. H.; Jang, J. Narrow Gap Filling in 25 Nm Shallow Trench Isolation Using Highly Porous Organosilica. *Thin Solid Films* **2014**, *562*, 166–171. https://doi.org/10.1016/j.tsf.2014.04.046.

[15] Park, J.; Wu, Z.; Park, J.; Kim, J.; Kuh, B.; Lee, J.; Hwang, S.; Han, S. Development of Reflow Fill of CGeSbTe Films for Sub-20 Nm Cells in 3D Cross-Point Memory. *Adv Materials Technologies* **2023**, *8* [1], 2200887. https://doi.org/10.1002/admt.202200887.

[16] Park, K. S.; Ni, Z.; Côté, A. P.; Choi, J. Y.; Huang, R.; Uribe-Romo, F. J.; Chae, H. K.; O'Keeffe, M.; Yaghi, O. M. Exceptional Chemical and Thermal Stability of Zeolitic Imidazolate Frameworks. *Proc. Natl. Acad. Sci. U.S.A.* **2006**, *103* [27], 10186–10191. https://doi.org/10.1073/pnas.0602439103.

[17] Perrot, V.; Roussey, A.; Benayad, A.; Veillerot, M.; Mariolle, D.; Solé-Daura, A.; Mellot-Draznieks, C.; Ricoul, F.; Canivet, J.; Quadrelli, E. A.; Jousseaume, V. ZIF-8 Thin Films by a Vapor-Phase Process: Limits to Growth. *Nanoscale* **2023**, *15* [15], 7115–7125. https://doi.org/10.1039/D3NR00404J.

[18] Siah, S. C.; Hoex, B.; Aberle, A. G. Accurate Characterization of Thin Films on Rough Surfaces by Spectroscopic Ellipsometry. *Thin Solid Films* **2013**, *545*, 451–457. https://doi.org/10.1016/j.tsf.2013.07.067.

[19] Smets, J.; Cruz, A. J.; Rubio-Giménez, V.; Tietze, M. L.; Kravchenko, D. E.; Arnauts, G.; Matavž, A.; Wauteraerts, N.; Tu, M.; Marcoen, K.; Imaz, I.; Maspoch, D.; Korytov, M.; Vereecken, P. M.; De Feyter, S.; Hauffman, T.; Ameloot, R. Molecular Layer Deposition of Zeolitic Imidazolate Framework-8 Films. *Chem. Mater.* **2023**, *35* [4], 1684–1690. https://doi.org/10.1021/acs.chemmater.2c03439.

[20] Stassen, I.; Burtch, N.; Talin, A.; Falcaro, P.; Allendorf, M.; Ameloot, R. An Updated Roadmap for the Integration of Metal–Organic Frameworks with Electronic Devices and Chemical Sensors. *Chem. Soc. Rev.* **2017**, *46* [11], 3185–3241. https://doi.org/10.1039/C7CS00122C.

[21] Stassen, I.; Styles, M.; Grenci, G.; Gorp, H. V.; Vanderlinden, W.; Feyter, S. D.; Falcaro, P.; Vos, D. D.; Vereecken, P.; Ameloot, R. Chemical Vapour Deposition of Zeolitic Imidazolate Framework Thin Films. *Nature Mater* **2016**, *15* [3], 304–310. https://doi.org/10.1038/nmat4509.

[22] Su, P.; Tu, M.; Ameloot, R.; Li, W. Vapor-Phase Processing of Metal–Organic Frameworks. *Acc. Chem. Res.* **2022**, *55* [2], 186–196. https://doi.org/10.1021/acs.accounts.1c00600.

[23] Usman, M.; Mendiratta, S.; Lu, K.-L. Metal-Organic Frameworks: New Interlayer Dielectric Materials. *CHEMELECTROCHEM* **2015**, *2* [6], 786–788. https://doi.org/10.1002/celc.201402456.

[24] Wheeler, D.; Josell, D.; Moffat, T. P. Modeling Superconformal Electrodeposition Using The Level Set Method. *J. Electrochem. Soc.* **2003**, *150* [5], C302. https://doi.org/10.1149/1.1562598.

[25] Zagorodniy, K.; Seifert, G.; Hermann, H. Metal-Organic Frameworks as Promising Candidates for Future Ultralow-k Dielectrics. *Appl. Phys. Lett.* **2010**, *97* [25], 251905. https://doi.org/10.1063/1.3529461.